PLOS | ONE

RESEARCH ARTICLE

Insulin Resistance Is Not Associated with an Impaired Mitochondrial Function in Contracting Gastrocnemius Muscle of Goto-Kakizaki Diabetic Rats *In Vivo*

Michael Macia[1]*, Emilie Pecchi[1], Christophe Vilmen[1], Martine Desrois[1], Carole Lan[1], Bernard Portha[2], Monique Bernard[1], David Bendahan[1], Benoît Giannesini[1]

1 Aix-Marseille Université, CNRS, CRMBM UMR 7339, 13385, Marseille, France, **2** Universitx Paris-Diderot, Sorbonne Paris Cité, Laboratoire B2PE, Unité BFA, CNRS EAC 4413, Paris, France

* michael.macia@live.fr

Citation: Macia M, Pecchi E, Vilmen C, Desrois M, Lan C, Portha B, et al. (2015) Insulin Resistance Is Not Associated with an Impaired Mitochondrial Function in Contracting Gastrocnemius Muscle of Goto-Kakizaki Diabetic Rats *In Vivo*. PLoS ONE 10 (6): e0129579. doi:10.1371/journal.pone.0129579

Academic Editor: Guillermo López Lluch, Universidad Pablo de Olavide, Centro Andaluz de Biología del Desarrollo-CSIC, SPAIN

Received: January 28, 2015

Accepted: May 11, 2015

Published: June 9, 2015

Data Availability Statement: All relevant data are within the paper.

Funding: These authors have no support or funding to report.

Competing Interests: The authors have declared that no competing interests exist.

Abstract

Insulin resistance, altered lipid metabolism and mitochondrial dysfunction in skeletal muscle would play a major role in type 2 diabetes mellitus (T2DM) development, but the causal relationships between these events remain conflicting. To clarify this issue, gastrocnemius muscle function and energetics were investigated throughout a multidisciplinary approach combining *in vivo* and *in vitro* measurements in Goto-Kakizaki (GK) rats, a non-obese T2DM model developing peripheral insulin resistant without abnormal level of plasma non-esterified fatty acids (NEFA). Wistar rats were used as controls. Mechanical performance and energy metabolism were assessed strictly non-invasively using magnetic resonance (MR) imaging and 31-phosphorus MR spectroscopy (^{31}P-MRS). Compared with control group, plasma insulin and glucose were respectively lower and higher in GK rats, but plasma NEFA level was normal. In resting GK muscle, phosphocreatine content was reduced whereas glucose content and intracellular pH were both higher. However, there were not differences between both groups for basal oxidative ATP synthesis rate, citrate synthase activity, and intramyocellular contents for lipids, glycogen, ATP and ADP (an important *in vivo* mitochondrial regulator). During a standardized fatiguing protocol (6 min of maximal repeated isometric contractions electrically induced at a frequency of 1.7 Hz), mechanical performance and glycolytic ATP production rate were reduced in diabetic animals whereas oxidative ATP production rate, maximal mitochondrial capacity and ATP cost of contraction were not changed. These findings provide *in vivo* evidence that insulin resistance is not caused by an impairment of mitochondrial function in this diabetic model.

Introduction

Type 2 diabetes mellitus (T2DM) is a metabolic disorder characterized by chronic hyperglycemia leading to long-term damage, dysfunction and failure of various organs, especially

pancreas, heart, skeletal muscle and blood vessels. T2DM is initially caused by peripheral insulin resistance syndrome, i.e., the inability of insulin to stimulate glucose absorption in peripheral tissue, in association with the progressive failure of the pancreatic cells to supply a sufficient amount of insulin [1]. The development of insulin resistance is itself caused by marked disturbances in insulin signaling induced by excess intake of carbohydrates and fats [2].

It is noteworthy that skeletal muscle plays a predominant role in the development of insulin resistance because it is one of the major organs participating in the assimilation, storage and utilization of glucose provided by food [3]. Insulin resistance causes in return a reduction of both exercise tolerance and mechanical performance [4]. Lipid metabolism alteration and mitochondrial dysfunction in skeletal muscle have been implicated in the etiology of T2DM but the causal relationships with insulin resistance development are still unclear [5–8]. Lipid oxidation has been reported to be increased in the early stage of insulin resistant state [9] while increased non-esterified fatty acids (NEFA) plasma level would inhibit skeletal muscle glucose uptake and glycogen synthesis [10]. Further, it has been clearly disclosed that the increase in intramyocellular lipids (IMCL) content reduces insulin sensitivity [11–13]. Besides, a link between mitochondrial function impairment and insulin resistance development is highly suspected [7]. On the basis of biochemical [14–16], gene expression [17, 18] and *in vivo* 31-phosphorus magnetic resonance spectroscopy (^{31}P-MRS) [7, 8, 19, 20] measurements, it has been initially proposed that mitochondrial capacity reduction contributes to IMCL accumulation thereby leading to insulin signaling failure and insulin resistance development. For instance, Bonnard et al. [21] compared mitochondrial density in mice receiving a high-fat-high-sucrose diet (HFHSD) and KKAγ mice, a genetic model of obesity and diabetes with a normal plasmatic NEFA. Interestingly, mitochondrial density and structure were abnormal only in the HFHSD model but not in the KKAγ strain, thereby suggesting a direct link between the increased plasmatic NEFA level and the mitochondrial number and integrity [21].

On the contrary, a growing number of studies has proposed that mitochondrial impairment is not the causative factor of insulin resistance development [22–27]. In a recent review, Holloszy [25] underlined that mitochondrial biogenesis increases in rodents receiving a high-fat diet, and mitochondrial deficiency severe enough to impair fat oxidation in resting muscle causes an increase, not a decrease, in insulin action. Overall, the causal link between mitochondrial function and lipid metabolism in the context of T2DM is still a matter of debate. However, it is noteworthy that most of the studies mentioned above have investigated mitochondrial density and enzymes activity but not mitochondrial function *per se*. Under these conditions, energy requirement is minimal and regulatory mechanisms of energy production have not been investigated. Data regarding *in vivo* mitochondrial function under conditions of high-energy demand such as in exercising muscle are then missing.

The purpose of the present study was to investigate mitochondrial function in electrically stimulated muscle of diabetic GK rat, a non-obese T2DM model displaying insulin resistance and normal NEFA plasmatic level [28–32]. Metabolic fluxes were measured strictly non-invasively with respect to mechanical performance using magnetic resonance (MR) imaging and ^{31}P-MRS, and mitochondrial content was evaluated on the basis of citrate synthase activity. The corresponding results were analyzed together with measurement of plasmatic levels of insulin, glucose and NEFA, IMCL and intramuscular contents for ATP, glycogen and glucose.

Materials and Methods

Animal care and feeding

Wistar (WT; $n = 8$) and Goto-Kakizaki [GK/Par subline [33]] ($n = 10$) 7-month-old male rats were used for these experiments. All animal work and care were carried out in strict accordance

with the guidelines of the European Communities Council Directive 86/609/EEC for Care and Use of Laboratory Animals with the approval of the animal experiment committee of Aix-Marseille University. Animals were socially housed as 2–3 per cage in an environmentally controlled facility (12–12 h light-dark cycle, 22°C) with free access to commercial standard food (diet 113; SAFE, Augy, France) and water until the time of the experiment. Every attempt was made to minimize the number and the suffering of animals.

In vivo investigation of gastrocnemius muscle function and energetics

Animal preparatio. Rats were initially anesthetized in an induction chamber with 4% isoflurane (Forene; Abbott France, Rungis, France) mixed in 33% O_2 (0.5 L/min) and 66% N_2O (1 L/min). The right lower hindlimb was shaved and electrode cream was applied at the knee and heel levels in order to optimize transcutaneous electrical stimulation. Anesthetized animal was placed supine in a home-built cradle allowing the strictly non-invasive MR investigation of gastrocnemius muscle function and energetics [34]. Briefly, the setup integrates an ergometer consisting of a foot pedal coupled to a force transducer, and two rod-shaped transcutaneous surface electrodes (located above the knee and at the heel level, respectively) connected to an electrical stimulator (Type 215/T; Harvard Apparatus, Germany). Corneas were protected from drying by applying ophthalmic cream and animal's head was placed in a facemask continuously supplied with 2.5% isoflurane in 33% O_2 (0.2 L/min) and 66% N_2O (0.4 L/min) throughout the experiment. The facemask was connected to an open-circuit gas anesthesia machine (Isotec 3, Ohmeda Medical, Herts, UK). Exhaled and excess gases were removed through a canister filled with activated charcoal (Smiths Industries Medical System, London, UK) mounted on an electrical pump extractor (Equipement Vétérinaire Minerve, France). The hindlimb was centered inside a 30 mm-diameter ^{1}H-MR Helmholtz imaging coil so that the belly of the gastrocnemius muscle located above an elliptic (10 x 16 mm) ^{31}P-MRS surface coil and the foot was positioned on the pedal of the ergometer. The gastrocnemius muscle was passively stretched at rest by adjusting the pedal position, thereby modifying the angle between the foot and the lower hindlimb in order to produce a maximum isometric twitch tension in response to a supramaximal square wave pulses (1 ms duration; 6–8 mA). During experiment, animal body temperature was controlled and maintained within a physiological range during anesthesia, using a feedback loop including an electrical heating blanket (Prang+Partner AG, Pfungen, Switzerland), a temperature control unit (Ref. No. 507137, Harvard Apparatus, Les Ulis, France) and a rectal probe (Ref. No. 507145, Harvard Apparatus, Les Ulis, France).

Muscle electrostimulation protocol and force output measurement. Mechanical performance was assessed during a standardized fatiguing protocol consisting in 6 min of repeated maximal isometric contractions induced electrically with square-wave pulses (6–8 mA, 1 ms duration) at a frequency of 3.3 Hz. Electrical signal coming out from the ergometer was amplified with a home-built amplifier (Operational amplifier AD620; Analog Devices, Norwood, MA, USA; gain = 70 dB; bandwidth 0–5 kHz) and converted to a digital signal (PCI-6220; National Instrument, Austin, TX, USA) that was continuously monitored and recorded on a personal computer using the WinATS 6.5 software (Sysma, Aix-en-Provence, France). Absolute isometric force production was calculated by integrating the isometric tension (in N) with respect to time, and was expressed as tension-time integral (in N*s). Specific force was defined as the absolute force normalized by muscle volume calculated from hindlimb MR images.

MR data acquisition. MR explorations were done in the 4.7-Tesla horizontal magnet of a 47/30 Biospec Avance MR system (Bruker, Karlsruhe, Germany). Sixteen consecutive non-contiguous axial images (1 mm thickness, spaced 0.5 mm) were acquired across the resting lower hindlimb using a rapid acquisition relaxation-enhanced (RARE) sequence (8 echoes; effective

echo time = 49.3 ms; actual echo time = 16 ms; repetition time = 2000 ms; 30 x 32 mm field of view; 256 x 192 matrix size). ^{31}P-MR spectra (16 accumulations; 1.8 s repetition time; 8 kHz spectral width, 512 data points) from the gastrocnemius muscle region were continuously acquired during 6 min of rest, 6 min of electrostimulation (ES) and 16 min of post-ES recovery. MR data acquisition was gated to muscle ES in order to reduce potential motion artifacts due to contraction. A fully relaxed spectrum (12 scans, 20 s repetition time) was acquired at rest, followed by a total of 768 saturated free induction decays (FID) (1.875 s repetition time). The first 64 FIDs were acquired at rest and summed together. The next 192 FIDs were acquired during the ES period and were summed by packets of 32, allowing a temporal resolution of ~60 s. The remaining 512 FIDs were obtained during the post-ES recovery period and were summed as 7 packets of 32 FIDs followed by 3 packets of 64 FIDs and one packet of 96 FIDs.

MR data processing. MR data were processed using a custom-written image analysis program developed with the IDL software (Interactive Data Language, Research System, Inc., Boulder, CO, USA). For each MR image, regions of interest were manually outlined using the DISPIMAG software [35] so that the corresponding cross-sectional areas could be measured (Fig 1A). Gastrocnemius muscle volume was then calculated as the sum of the volumes included between the consecutive slices. Relative concentrations of phosphocreatine (PCr), inorganic phosphate (P_i) and β-ATP were obtained by a time-domain fitting routine using the AMARES-MRUI Fortran code [36] and appropriate prior knowledge of the ATP multiplets. Signal areas were corrected for magnetic saturation using fully relaxed spectra collected at rest with a repetition time of 20 s. Absolute concentrations of phosphorylated compounds were expressed relative to a resting β-ATP concentration determined by bioluminescence as detailed below. Intracellular pH (pH_i) was calculated from the chemical shift of the P_i relative to the PCr signal [37]. Time-points for the time course of phosphorylated metabolite concentrations and pH_i were assigned to the midpoint of the acquisition interval.

Metabolic fluxes calculations. ATP productions from the different pathways (PCr degradation via CK reaction, mitochondrial oxidative phosphorylation and glycolysis) were calculated as described previously [38–40]. ATP cost of contraction was calculated as the rate of ATP production scaled to force output during the same period of time.

ATP production rate from PCr degradation via creatine kinase (CK) reaction (D) was directly calculated using the [PCr] time-course throughout the stimulation period: $D = -dPCr/dt$.

Oxidative ATP production rate (Q) was calculated considering that ADP stimulates oxidative ATP synthesis throughout a hyperbolic relationship: $Q = Q_{max}/(1+K_m/[ADP])$, in which K_m (the ADP concentration at half-maximal oxidation rate) is 50 μM as previously reported in rat gastrocnemius muscle [41] and Q_{max} is the maximal oxidative capacity. [ADP] was calculated from [PCr], [ATP] and pH_i using the CK equilibrium constant ($K = 1.67\ 10^9\ M^{-1}$) [42]. Q_{max} was calculated using the rate of PCr resynthesis at the start of the post-stimulation recovery period (VPCr$_{rec}$) and the concentration of free cytosolic ADP measured at the end of the stimulation period: $Q_{max} = V\text{PCr}_{rec}\ (1 + K_m/[\text{ADP}]_{end})$. VPCr$_{rec}$ was the product of k (the pseudo-first-order rate-constant of PCr recovery) and $[\text{PCr}]_{cons}$ (the amount of PCr consumed at the end of the stimulation period). In order to determine k, the PCr time-course during the post-stimulation recovery period was fitted to a first-order exponential curve: $[\text{PCr}]_t = [\text{PCr}]_{rest} - [\text{PCr}]_{cons}\ e^{-kt}$, where $[\text{PCr}]_{rest}$ is the concentration of PCr measured at rest.

Glycolytic ATP production rate (L) was inferred considering that, when coupled to ATP hydrolysis, glycolytic ATP production is related to proton production (H_{Gly}) with a stoichiom try of 1.5 moles ATP per proton ($L = 1.5\ H_{Gly}$) [43]. This proton production can be calculated from the observed changes in pH_i and taking into account protons consumed by PCr degradation throughout the CK reaction (H_{CK}), passively buffered in the cytosol (H_β), leaving the cell (rate of net proton efflux, H_{Efflux}) and produced by oxidative phosphorylation

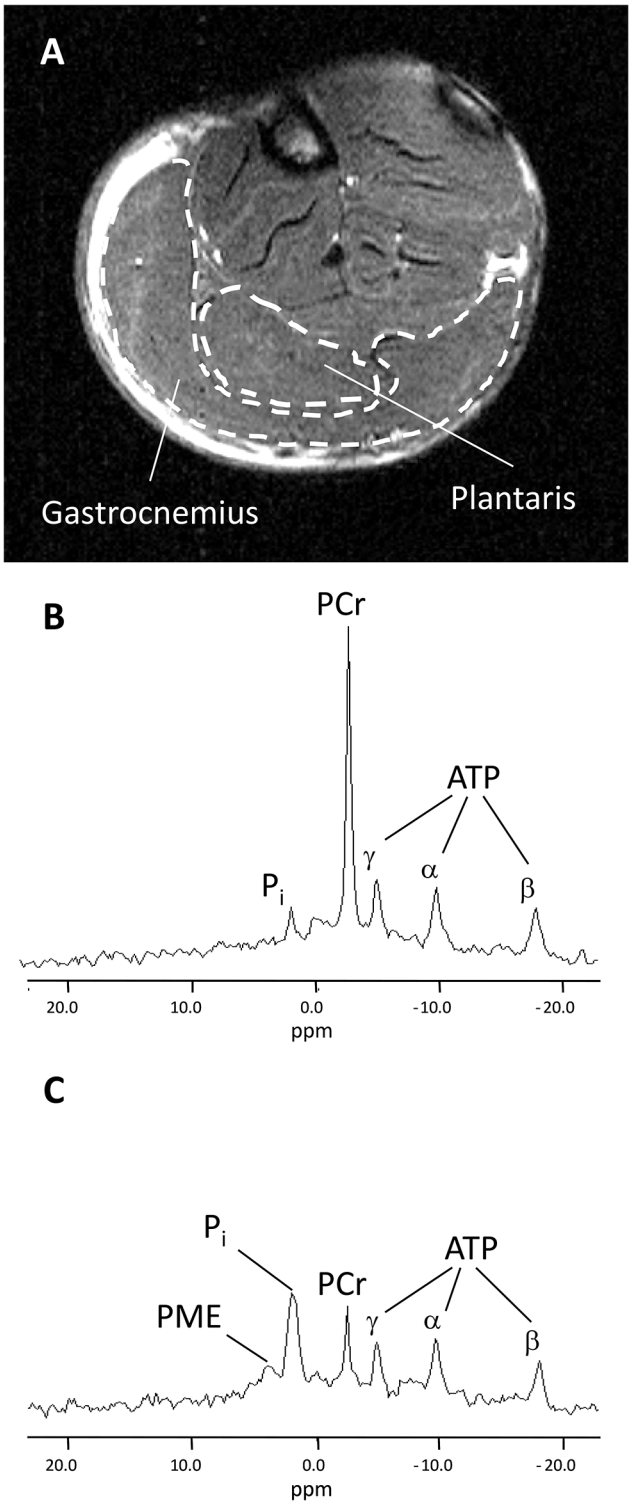

Fig 1. Typical transversal slice obtained by MRI of a rat lower hindlimb (A), ^{31}P-MRS spectra obtained from a single WT rat gastrocnemius muscle at rest (B) and at the end of 6-min of *in vivo* electrostimulation protocol (C). Abbreviations for signal assignments (in p.p.m.) are PME (phosphomonoester), P_i (inorganic phosphate), PCr (phosphocreatine), and γ-, α-, and β-resonances of ATP.

doi:10.1371/journal.pone.0129579.g001

(H_{Ox}): $H_{Gly} = H_{CK} + H_{\beta} + H_{Efflux} — H_{Ox}$. Calculation of H_{CK} was done from the time-dependent changes in [PCr] and with the stoichiometric coefficient $\varphi = 1/(1+10^{(pHi-6.75)})$, which represents the number of protons associated to P_i production [44]: $H_{CK} = \varphi\ dPCr/dt$. Besides, H_{β} was the product of β_{total} (in Slykes, millimoles acid added per unit change in pH_i) and pH_i changes ($\Delta pH_i = pH_{observed} — pH_{rest}$): $H_{\beta} = (-\beta_{total}\Delta pH_i)$. The apparent buffering capacity (β_{total}) takes into account the buffering capacity of P_i (β_{Pi}) and the buffering capacity of muscle tissue (β_{tissue}): $\beta_{total} = \beta_{Pi} + \beta_{tissue}$, where $\beta_{Pi} = 2.3[P_i]/((1+10^{(pHi-6.75)})(1+10^{(6.75-pHi)}))$ [44]. It has been shown that β_{tissue} varies linearly between pH 7 (16 Slykes) and pH 6 (37 Slykes) in murine gastrocnemius muscle [45]. Accordingly, β_{tissue} was calculated as follows: $\beta_{tissue} = -21pH_i+163$. During muscle stimulation, H_{efflux} was calculated using the proportionality constant λ (in μmol/s/pH unit) referring to the ratio between the rate of proton efflux and pH_i: $H_{efflux} = -\lambda\Delta pH_i$. This constant was determined at the start of the post-stimulation recovery period as $\lambda = -V_{eff}/\Delta pH_i$. At that time, although protons are generated throughout the aerobic PCr resynthesis, pH_i recovers back to basal because of net proton efflux from the cell: H_{efflux} can then be calculated taking into account proton loads associated with CK reaction and mitochondrial ATP synthesis on the one hand and the rate of pH changes on the other hand. $H_{efflux} = H_{CK} + H_{Ox} + \beta_{total}dpH_i/dt$. The rate of aerobic proton production coupled to oxidative ATP synthesis was quantified as follows [44]: $H_{Ox} = mVPCr_{rec}$, with $m = 0.16/(1+10^{(6.1-pH)})$.

In vitro analytical procedures

After MR experiments, transcardiac blood samples (0.25 ml) were obtained with a thin needle carefully introduced into the heart during the anesthetic epoch. Plasma was immediately separated after blood centrifugation (15 min at 4,000 rpm) in EDTA-treated tubes. Afterwards, anesthetized animals were immediately euthanized by cervical dislocation, and gastrocnemius muscles were quickly removed, freeze-clamped with liquid nitrogen-chilled metal tongs and stored at -80°C.

Plasmatic concentrations of insulin, glucose and NEFA were measured using insulin (Mercodia, Uppsala, Sweden), glucose (Randox Laboratories, Crumlin, Antrim, UK) and NEFA (Roche Diagnostics, Roche Applied Science, Mannheim, Germany) determination kits.

Intramuscular contents for ATP, glycogen and glucose were determined in freeze-clamped gastrocnemius muscles (50 to 60 mg) homogenized in ice-cold 0.6 M perchloric acid (1.2 ml) with a Polytron PT2100 (Kinematica AG, Luzern, Switzerland). After incubation for 15 min at 4°C, the homogenate was centrifuged (15 min, 2000 x *g*, 4°C) and the supernatant was neutralized with K_2CO_3 and placed for 30 min at 4°C. ATP concentration was measured using a bioluminescence-based determination kit (ref. A22066, Invitrogen, Eugene, Oregon, USA), and glycogen and glucose contents were assessed by colorimetric procedure (ref. E2GN-100, EnzyChrome, Hayward, California, USA).

IMCL content was determined in freeze-clamped gastrocnemius muscle (50 to 70 mg) homogenized in 1 ml of a 1% (w/v) Triton X-100 in chloroform solution. Briefly, homogenate was centrifuged (10 min, 13000 x *g*, 20°C), the organic phase was collected and the chloroform was removed using a nitrogen evaporator (N-EVAP-111, Organomation, Berlin, Massachusetts, USA). IMCL content was then measured using a colorimetric detection kit (ref. MAK044, Sigma-Aldrich, St. Louis, Missouri, USA).

Citrate synthase activity was measured (ref. CS0720, Sigma-Aldrich, St. Louis, Missouri, USA) in another part (20 to 30 mg) of the freeze-clamped muscle, which was homogenized with a lysis reagent (ref. C3228, Sigma-Aldrich, St. Louis, Missouri, USA) and a protease inhibitor cocktail (P8340, Sigma-Aldrich, St. Louis, Missouri, USA).

Table 1. Animal characteristics.

	WT	GK	*P*-value
Body weight (g)	491 ± 16	423 ± 4	< 0.001
Gastrocnemius muscle volume (cm^3)	1.84 ± 0.04	1.56 ± 0.02	< 0.001
BW/GV (g/cm^3)	268 ± 10	272 ± 3	n.s.
Plasma			
Insulin (ng/ml)	3.4 ± 0.3	2.2 ± 0.2	< 0.01
Glucose (mM)	10.9 ± 0.6	19.4 ± 1.9	< 0.001
NEFA (mM)	0.22 ± 0.02	0.21 ± 0.02	n.s
Gastrocnemius muscle			
Glycogen (μmol/g)	20.5 ± 1.4	20.2 ± 1.5	n.s.
Glucose (μmol/g)	8.1 ± 0.4	10.0 ± 0.7	0.031
IMCL (μmol/g)	1.8 ± 0.1	1.6 ± 0.1	n.s.

Data are means ± SEM; n.s., not statistically significant; BW/GV, body weight/gastrocnemius muscle volume ratio.

doi:10.1371/journal.pone.0129579.t001

Statistical analysis

Data were analyzed with JMP software (SAS Institute Inc., Cary, North Carolina, USA). For variables changing with respect to time during ES and post-ES recovery periods, overall time-courses were analyzed with two-way (group x time) analyses of variance (ANOVAs) with repeated measures on time. When appropriate, post-hoc Tukey tests were used in order to identify differences at each time-point. Other variables were compared using unpaired two-tailed Student's t-test. $P < 0.05$ was considered as significant. Values are presented as means ± SE.

Results

Animal characteristics

The corresponding data are summarized in Table 1. Body weight and gastrocnemius muscle volume were lower (-14% and -15%, respectively) in GK rats, but body weight-to-gastrocnemius volume ratio was similar between both groups. Plasmatic and muscle glucose contents were higher (+79% and +23%, respectively) in GK animals whereas plasma insulin was lower (-37%). On the other hand, there were no differences between both groups for NEFA, IMCL and intramuscular glycogen contents.

Mechanical performance

For GK and WT animals, both absolute and specific force displayed a biphasic profile with an initial transient increase in the early stage of the 6-min ES period followed by a progressive decrease until the end of the ES protocol as a sign of fatigue development (Fig 2A and 2B). At this stage, the extent of force reduction was significantly lower (-14%) in GK animals. Overall, the total absolute and specific force developed during the whole 6-min ES period were both lower (-34% and -22%, respectively) in the GK group (Fig 2C and 2D).

Metabolic changes

Typical ^{31}P-MR spectra recorded from a single WT gastrocnemius muscle are presented in Fig 1B and 1C. At rest, [PCr] and PCr/ATP ratio were lower (-23% and -21%, respectively) in the GK group whereas pH_i was higher (Table 2). On the other hand, there were no differences between both groups for [ATP], [ADP] and citrate synthase activity (Table 2).

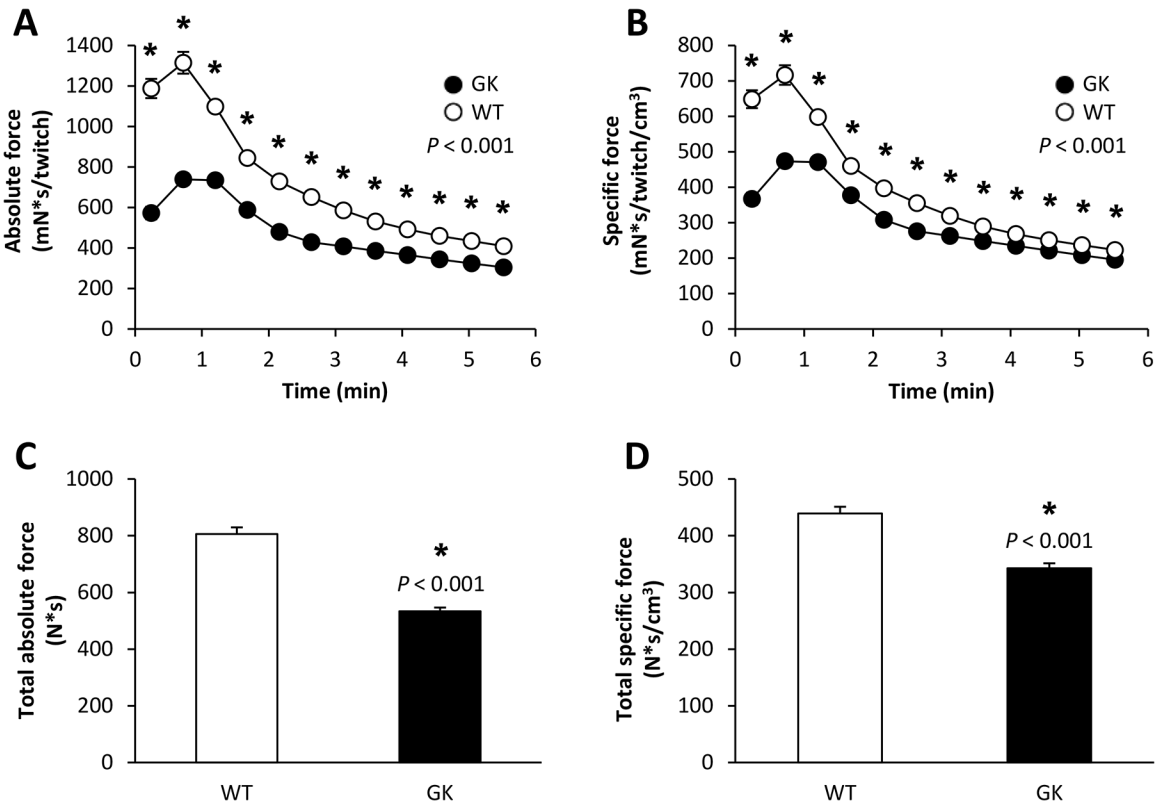

Fig 2. Time-dependent changes in absolute (A) and specific (B) force during the 6-min *in vivo* electrostimulation protocol, total amount of absolute (C) and specific (D) force produced during the whole protocol. Values are means ± SEM. *Significant difference between GK and WT.

doi:10.1371/journal.pone.0129579.g002

At the onset of the ES protocol, PCr was rapidly consumed (Fig 3A) at an initial rate that was significantly lower in the GK group (Table 2). Afterward, PCr level reached a steady state that was maintained until the end of the ES period. At this time, the extent of PCr consumption (ΔPCr) was 25% lower in the GK group (Table 2). During the first 3 minutes of the ES period, pH_i fell rapidly to reach a steady state that was fairly constant during the remaining ES period (Fig 3B). The extent of acidosis (ΔpH_i) at the end of the ES period was similar between both groups (Table 2). For each group, ATP level decreased linearly throughout the ES protocol, but to a lower extent in GK animals ($P < 0.005$, Fig 3C).

During the post-ES recovery period, phosphorylated compounds and pH_i progressively reached their respective basal values (Fig 3). The maximal oxidative capacity (Q_{max}) and both the initial rate ($VPCr_{rec}$) and rate constant ($kPCr_{rec}$) of PCr resynthesis were similar in GK and control groups (Table 2).

Metabolic fluxes and ATP cost of contraction

The time-courses of ATP production rates from CK reaction and oxidative phosphorylation throughout the 6-min ES period did not differ between both groups (Fig 4A and 4B). On the other hand, glycolytic ATP production rate in the early stage of the ES protocol was lower in GK animals (Fig 4C). Overall, the total rate of ATP production (calculated as the sum of ATP produced by the three metabolic pathways over the whole ES protocol) was similar between GK and WT rats (Fig 4D). Besides, the average ATP cost of contraction (calculated across the

Table 2. Energy metabolism of gastrocnemius muscle.

	WT	GK	*P*-value
Rest			
[PCr]/[ATP]	4.4 ± 0.2	3.5 ± 0.2	0.005
PCr (μmol/g)	32 ± 2	24 ± 1	0.002
ATP (μmol/g)	7.22 ± 0.04	7.06 ± 0.4	n.s.
ADP (nmol/g)	8.8 ± 0.2	10.4 ± 0.7	n.s.
pH_i	7.06 ± 0.01	7.14 ± 0.03	0.026
Citrate synthase activity (mmol/g/min)	0.27 ± 0.04	0.24 ± 0.03	n.s.
Onset of the stimulation period			
$VPCr_{stim}$ (μmol/g/min)	63 ± 4	37 ± 3	< 0.001
$kPCr_{stim}$ (min^{-1})	2.4 ± 0.1	2.2 ± 0.2	n.s.
End of the stimulation period			
PCr (μmol/g)	7 ± 1	10 ± 1	0.031
ΔPCr_{cons} (%)	78 ± 1	58 ± 4	< 0.001
ADP (nmol/g)	23 ± 1	21 ± 2	n.s.
pH_i	6.34 ± 0.03	6.41 ± 0.03	n.s.
ΔpH_i (pH units)	0.72 ± 0.03	0.73 ± 0.04	n.s.
Recovery			
$VPCr_{rec}$ (μmol/g/min)	8 ± 1	6 ± 1	n.s.
$kPCr_{rec}$ (min^{-1})	0.38 ± 0.04	0.39 ± 0.04	n.s.
Q_{max} (μmol/g/min)	26 ± 4	22 ± 3	n.s.

Data are means ± SEM; n.s., not statistically significant; $VPCr_{stim}$, initial rate of PCr breakdown at the start of the 6-min stimulation period; $kPCr_{stim}$, PCr breakdown rate constant at the start of the 6-min stimulation period; ΔPCr_{cons}, PCr consumption at the end of 6-min stimulation period; $VPCr_{rec}$, initial rate of PCr resynthesis at the start of the post-stimulation period; $kPCr_{rec}$, PCr resynthesis rate constant at recovery period start; Q_{max}, maximal oxidative capacity.

doi:10.1371/journal.pone.0129579.t002

whole 6-min ES period as the total amount of ATP production scaled to the total force output during the same period) did not differ between GK and Wistar rats (Fig 5).

Discussion

The causative relationships between insulin-resistance, mitochondrial dysfunction and lipid metabolism alteration are still a matter of debate. The GK model is of interest in order to address this issue given that it is a non-obese T2DM model displaying a normal NEFA plasmatic level and an insulin-resistance [28–32]. Although this model has been widely used for the study of T2DM, data regarding the *in vivo* mitochondrial function are very scarce.

In agreement with previous studies, we found increased plasmatic glucose and decreased insulin level in GK rats whereas both NEFA and IMCL levels were unaltered [30, 46]. These findings are in line with the view that this model exhibits a moderate but stable fasting hyperglycemia early in life and develops beta-cells failure with increasing age, thereby reducing the insulin secretion [29] and leading to insulin resistant state [47, 48].

Our data clearly showed that energy metabolism was disturbed in resting GK muscle. In particular, PCr/ATP ratio and PCr content were both lower, whereas ATP level was unchanged. PCr is considered to play a crucial role in cellular energy metabolism [49]. Actually, PCr level is under the control of creatine kinase (CK), which transfers high-energy phosphate from PCr to ADP to form ATP (via the reaction: $PCr + ADP + H^+ \leftrightarrow ATP + creatine$) and the PCr-CK system is involved (i) in energy buffering in order to maintain ATP pool charged and

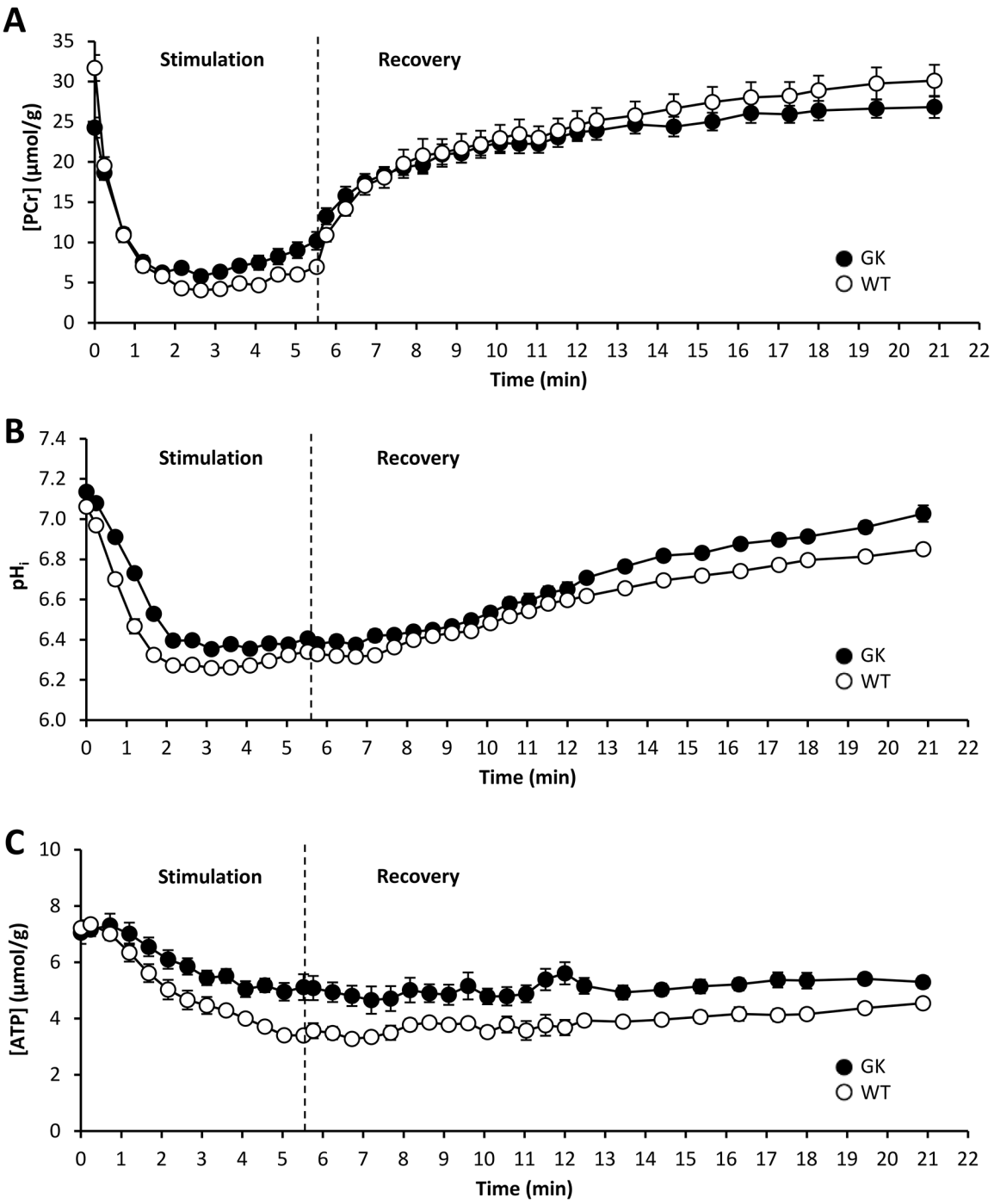

Fig 3. Time-dependent changes in gastrocnemius muscle [PCr] (A), intracellular pH (B) and [ATP] (C) during 6 min of *in vivo* electrostimulation and 15 min of post-electrostimulation recovery periods. The first point (t = 0) indicates the measured value during the resting period. Values are means ± SEM.

doi:10.1371/journal.pone.0129579.g003

(ii) in high-energy phosphate transport between the site of production (mitochondria) and utilization of ATP. Thus, the reduction of PCr content reported herein could indicate that ATP homeostasis was preserved in GK muscle at the expense of PCr stores in order to ensure the basal energy demand. Considering that ATP generation is mainly aerobic at rest [50], these

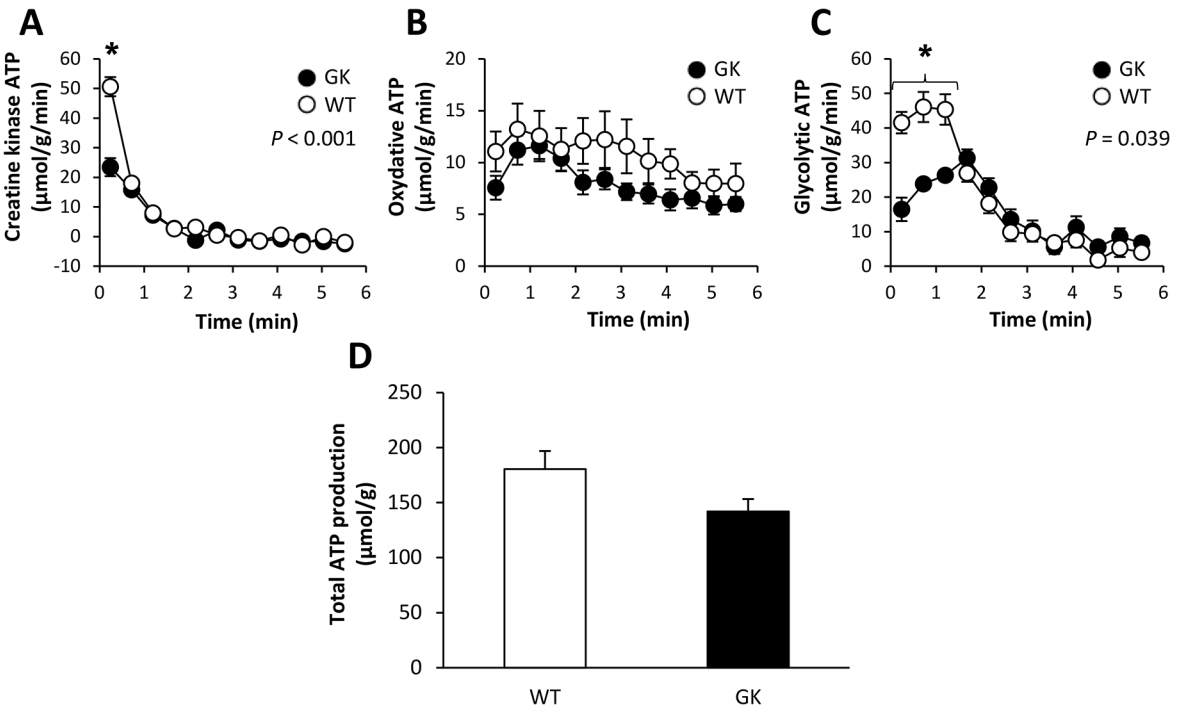

Fig 4. Rates of ATP production from CK reaction (A), oxidative phosphorylation (B) and glycolysis (C) during the 6-min in vivo electrostimulation protocol and total rate of ATP produced the whole protocol (D). Values are means ± SEM. *Significant difference between GK and WT.

doi:10.1371/journal.pone.0129579.g004

findings might suggest an impaired mitochondrial ATP generation. However, neither of the results we obtained *in vivo* (^{31}P-MRS) or *in vitro* (citrate synthase activity assays) support any reduction in mitochondrial capacity, which is consistent with the unaffected mitochondrial respiration reported in isolated mitochondria from GK rat quadriceps muscle [51]. On that basis, the reduced basal PCr content would not be linked to an impaired mitochondrial function. Besides, a decline in basal PCr content has been previously observed as the result of muscle ischemia in association with intracellular acidosis [52]. Interestingly, *in situ* microscopy experiments have reported a disturbed muscle microcirculation in the *spinotrapezius* muscle of GK rats, hence leading to reduced delivery and transport of oxygen [53]. Nevertheless, any

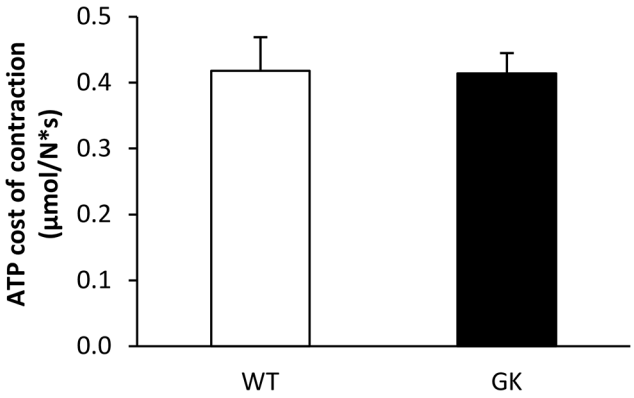

Fig 5. Averaged ATP cost of contraction during the 6-min electrostimulation protocol. Values are means ± SEM.

doi:10.1371/journal.pone.0129579.g005

disturbed oxygen supply can be dismissed in the present study given that we did not observe a concomitant acidosis in the gastrocnemius muscle but on the contrary a basal alkalosis. On the other hand, considering that ADP stimulates mitochondrial ATP generation through a feedback loop [38] and basal [ADP] was similar in both groups, PCr content reduction we measured in GK muscle could be interpreted as a compensatory mechanism aiming at keeping [ADP] constant in the face of the increased pH_i in order to maintain a normal mitochondrial function.

However, the fact that ATP level and mitochondrial function were not altered in resting GK muscle does not necessarily imply that oxidative capacity was preserved in working muscle, i.e., when energy demand may increase substantially. As compared to rest, muscle energy demand can actually increase by several orders of magnitude in exercising muscle in order to maintain ATP homeostasis [54]. In the present study, we implemented an intense fatiguing protocol consisting in 6-min of repeated maximal isometric contractions to produce wide changes in metabolic and mechanical changes. Despite this, we did not measure any alteration of oxidative ATP production in contracting GK muscle. Moreover, the maximal oxidative capacity and the initial rate of post-electrostimulation PCr resynthesis–an *in vivo* index of mitochondrial function [55]–did not differ between both groups thereby indicating that mitochondrial function was not altered in the GK model.

It must be pointed out that the rate of glycolytic ATP production in the early stage of the electrostimulation period was significantly lower in GK muscle. One can assume that this lower rate was linked to the reduced glucose uptake already observed in skeletal muscle of insulin resistant and diabetic patients [56]. This assumption appears however unlikely herein considering the unaltered glycogen content and the even higher glucose content in the GK rats gastrocnemius muscle. The decreased glycolytic flux could rather be related to decreased glucose utilization. In the diabetic state, glucose is indeed preferentially catabolized into the polyol pathway away from energy-producing glycolysis as a result of a reduced glyceraldehydes 3-phosphate dehydrogenase (GAPDH) reaction kinetics and other downstream reactions, e.g., enolase and pyruvate kinase [57].

Another interesting result is that mechanical performance was reduced in GK rats. The lower (-34%) absolute force developed throughout the fatiguing protocol is in line with the reduced muscle strength observed in diabetic patients [4]. Interestingly, this lower force-generating capacity was not fully accounted by the smaller size of the GK gastrocnemius muscle measured from anatomic MR images. Indeed, specific force (i.e., absolute force scaled to muscle size) was also reduced in the diabetic animals, but to a lower extent (-22%), which indicates that additional mechanisms are involved in the impairment of muscle performance. Limitation of energy supply is considered to play a major role in the failure of muscle to sustain force [58], but such an issue is unlikely in contracting GK muscle given that we found that throughout the whole electrostimulation period, ATP level did not fall down to any critical threshold and was even higher than the corresponding level in Wistar rats, hence indicating that the rate of ATP regeneration was not compromised. Further, it can be dismissed that a proportion of ATP produced in contracting GK muscle would be wasted in non-contractile processes because we found that ATP cost of contraction, i.e., the contractile efficiency, was not altered in these animals. Our findings might be at a first glance considered as opposite to that of a previous calorimetric study showing that basal energy expenditure is increased in patients with congenital insulin resistance [59]. Nevertheless, it must be kept in mind that this increased energy expenditure was measured at rest at the whole body level, and might differ from the results we obtained at the skeletal muscle level. Besides, an attractive explanation for the reduced mechanical performance would rather lie in the diabetic neuropathy previously reported in GK model [60]. This nerve disorder causes indeed motor dysfunction leading to muscle weakness

and atrophy [61–63]. Diabetic neuropathy could further, in combination to increased autophagy already reported in this model [64], explains the smaller size of gastrocnemius muscle we reported herein.

In conclusion, oxidative ATP generation capacity at rest and during sustained fatiguing electrostimulation protocol was not altered in the GK rat model. These findings provide *in vivo* evidence that insulin resistance is not caused by a primary defect in mitochondrial function in this diabetic model.

Acknowledgments

M.M., B.G., D.B. and C.V. contributed to the conception and the design of the research; B.G. and M.M. performed the experiments; E.P. and C.L. contributed to the *in vitro* assessments; M. M. analyzed the data; B.G. and M.M. interpreted the results of the experiments; M.M. prepared the figures; M.M. drafted the manuscript; B.G., D.B. and M.M. contributed to discussion, and reviewed and edited manuscript. M.M., E.P., C.V., C.L., M.D., B.P., M.B., D.B. and B.G. approved the final version of the manuscript.

B.G. is the guarantor of this work and, as such, had full access to all the data in the study and takes responsibility for the integrity of the data and the accuracy of the data analysis.

Author Contributions

Conceived and designed the experiments: MM BG DB CV. Performed the experiments: MM BG. Analyzed the data: MM. Contributed reagents/materials/analysis tools: EP CL CV. Wrote the paper: MM BG DB. Approved the manuscript: MD BP MB.

References

1. Fraenkel M, Ketzinel-Gilad M, Ariav Y, Pappo O, Karaca M, Castel J, et al. mTOR inhibition by rapamycin prevents beta-cell adaptation to hyperglycemia and exacerbates the metabolic state in type 2 diabetes. Diabetes. 2008; 57(4):945–57. Epub 2008/01/05. doi: 10.2337/db07-0922 db07-0922 [pii]. PubMed PMID: 18174523.
2. Um SH, D'Alessio D, Thomas G. Nutrient overload, insulin resistance, and ribosomal protein S6 kinase 1, S6K1. Cell Metab. 2006; 3(6):393–402. Epub 2006/06/07. S1550-4131(06)00158-6 [pii] doi: 10.1016/j.cmet.2006.05.003 PMID: 16753575.
3. Reaven GM. Banting lecture 1988. Role of insulin resistance in human disease. Diabetes. 1988; 37 (12):1595–607. Epub 1988/12/01. PMID: 3056758.
4. Andreassen CS, Jakobsen J, Flyvbjerg A, Andersen H. Expression of neurotrophic factors in diabetic muscle—relation to neuropathy and muscle strength. Brain. 2009; 132(Pt 10):2724–33. Epub 2009/08/22. awp208 [pii] doi: 10.1093/brain/awp208 PMID: 19696031.
5. Rabol R, Boushel R, Dela F. Mitochondrial oxidative function and type 2 diabetes. Appl Physiol Nutr Metab. 2006; 31(6):675–83. Epub 2007/01/11. h06-071 [pii] doi: 10.1139/h06-071 PMID: 17213881.
6. Lowell BB, Shulman GI. Mitochondrial dysfunction and type 2 diabetes. Science. 2005; 307 (5708):384–7. Epub 2005/01/22. 307/5708/384 [pii] doi: 10.1126/science.1104343 PMID: 15662004.
7. Petersen KF, Befroy D, Dufour S, Dziura J, Ariyan C, Rothman DL, et al. Mitochondrial dysfunction in the elderly: possible role in insulin resistance. Science. 2003; 300(5622):1140–2. Epub 2003/05/17. doi: 10.1126/science.1082889 300/5622/1140 [pii]. PMID: 12750520; PubMed Central PMCID: PMC3004429.
8. Petersen KF, Dufour S, Befroy D, Garcia R, Shulman GI. Impaired mitochondrial activity in the insulin-resistant offspring of patients with type 2 diabetes. N Engl J Med. 2004; 350(7):664–71. Epub 2004/02/13. doi: 10.1056/NEJMoa031314 350/7/664 [pii]. PMID: 14960743; PubMed Central PMCID: PMC2995502.
9. Groop LC, Bonadonna RC, Simonson DC, Petrides AS, Shank M, DeFronzo RA. Effect of insulin on oxidative and nonoxidative pathways of free fatty acid metabolism in human obesity. Am J Physiol. 1992; 263(1 Pt 1):E79–84. Epub 1992/07/01. PMID: 1636701.

10. Roden M, Price TB, Perseghin G, Petersen KF, Rothman DL, Cline GW, et al. Mechanism of free fatty acid-induced insulin resistance in humans. J Clin Invest. 1996; 97(12):2859–65. Epub 1996/06/15. doi: 10.1172/JCI118742 PMID: 8675698; PubMed Central PMCID: PMC507380.

11. Pan DA, Lillioja S, Kriketos AD, Milner MR, Baur LA, Bogardus C, et al. Skeletal muscle triglyceride levels are inversely related to insulin action. Diabetes. 1997; 46(6):983–8. Epub 1997/06/01. PMID: 9166669.

12. Phillips DI, Caddy S, Ilic V, Fielding BA, Frayn KN, Borthwick AC, et al. Intramuscular triglyceride and muscle insulin sensitivity: evidence for a relationship in nondiabetic subjects. Metabolism. 1996; 45 (8):947–50. Epub 1996/08/01. PMID: 8769349.

13. Krssak M, Falk Petersen K, Dresner A, DiPietro L, Vogel SM, Rothman DL, et al. Intramyocellular lipid concentrations are correlated with insulin sensitivity in humans: a 1H NMR spectroscopy study. Diabetologia. 1999; 42(1):113–6. Epub 1999/02/23. doi: 10.1007/s001250051123 PMID: 10027589.

14. He J, Watkins S, Kelley DE. Skeletal muscle lipid content and oxidative enzyme activity in relation to muscle fiber type in type 2 diabetes and obesity. Diabetes. 2001; 50(4):817–23. Epub 2001/04/06. PMID: 11289047.

15. Kelley DE, He J, Menshikova EV, Ritov VB. Dysfunction of mitochondria in human skeletal muscle in type 2 diabetes. Diabetes. 2002; 51(10):2944–50. Epub 2002/09/28. PMID: 12351431.

16. Ritov VB, Menshikova EV, He J, Ferrell RE, Goodpaster BH, Kelley DE. Deficiency of subsarcolemmal mitochondria in obesity and type 2 diabetes. Diabetes. 2005; 54(1):8–14. Epub 2004/12/24. 54/1/8 [pii]. PMID: 15616005.

17. Mootha VK, Lindgren CM, Eriksson KF, Subramanian A, Sihag S, Lehar J, et al. PGC-1alpha-responsive genes involved in oxidative phosphorylation are coordinately downregulated in human diabetes. Nat Genet. 2003; 34(3):267–73. Epub 2003/06/17. doi: 10.1038/ng1180 ng1180 [pii]. PMID: 12808457.

18. Patti ME, Butte AJ, Crunkhorn S, Cusi K, Berria R, Kashyap S, et al. Coordinated reduction of genes of oxidative metabolism in humans with insulin resistance and diabetes: Potential role of PGC1 and NRF1. Proc Natl Acad Sci U S A. 2003; 100(14):8466–71. Epub 2003/07/02. doi: 10.1073/pnas.1032913100 1032913100 [pii]. PMID: 12832613; PubMed Central PMCID: PMC166252.

19. Schrauwen-Hinderling VB, Kooi ME, Hesselink MK, Jeneson JA, Backes WH, van Echteld CJ, et al. Impaired in vivo mitochondrial function but similar intramyocellular lipid content in patients with type 2 diabetes mellitus and BMI-matched control subjects. Diabetologia. 2007; 50(1):113–20. Epub 2006/11/10. doi: 10.1007/s00125-006-0475-1 PMID: 17093944.

20. Befroy DE, Petersen KF, Dufour S, Mason GF, de Graaf RA, Rothman DL, et al. Impaired mitochondrial substrate oxidation in muscle of insulin-resistant offspring of type 2 diabetic patients. Diabetes. 2007; 56(5):1376–81. Epub 2007/02/09. db06-0783 [pii] doi: 10.2337/db06-0783 PMID: 17287462; PubMed Central PMCID: PMC2995532.

21. Bonnard C, Durand A, Peyrol S, Chanseaume E, Chauvin MA, Morio B, et al. Mitochondrial dysfunction results from oxidative stress in the skeletal muscle of diet-induced insulin-resistant mice. J Clin Invest. 2008; 118(2):789–800. Epub 2008/01/12. doi: 10.1172/JCI32601 PMID: 18188455; PubMed Central PMCID: PMC2176186.

22. Han DH, Hancock CR, Jung SR, Higashida K, Kim SH, Holloszy JO. Deficiency of the mitochondrial electron transport chain in muscle does not cause insulin resistance. PLoS One. 2011; 6(5):e19739. Epub 2011/05/19. doi: 10.1371/journal.pone.0019739 PONE-D-10-04908 [pii]. PMID: 21589859; PubMed Central PMCID: PMC3093385.

23. Hancock CR, Han DH, Chen M, Terada S, Yasuda T, Wright DC, et al. High-fat diets cause insulin resistance despite an increase in muscle mitochondria. Proc Natl Acad Sci U S A. 2008; 105(22):7815–20. Epub 2008/05/30. doi: 10.1073/pnas.0802057105 0802057105 [pii]. PMID: 18509063; PubMed Central PMCID: PMC2409421.

24. Holloszy JO. Skeletal muscle "mitochondrial deficiency" does not mediate insulin resistance. Am J Clin Nutr. 2009; 89(1):463S–6S. Epub 2008/12/06. doi: 10.3945/ajcn.2008.26717C ajcn.2008.26717C [pii]. PMID: 19056574.

25. Holloszy JO. "Deficiency" of mitochondria in muscle does not cause insulin resistance. Diabetes. 2013; 62(4):1036–40. Epub 2013/03/23. doi: 10.2337/db12-1107 62/4/1036 [pii]. PMID: 23520283; PubMed Central PMCID: PMC3609559.

26. Holloway GP, Bonen A, Spriet LL. Regulation of skeletal muscle mitochondrial fatty acid metabolism in lean and obese individuals. Am J Clin Nutr. 2009; 89(1):455S–62S. Epub 2008/12/06. doi: 10.3945/ajcn.2008.26717B ajcn.2008.26717B [pii]. PMID: 19056573.

27. Holloway GP, Gurd BJ, Snook LA, Lally J, Bonen A. Compensatory increases in nuclear PGC1alpha protein are primarily associated with subsarcolemmal mitochondrial adaptations in ZDF rats. Diabetes. 2010; 59(4):819–28. Epub 2010/01/28. doi: 10.2337/db09-1519 db09-1519 [pii]. PMID: 20103701; PubMed Central PMCID: PMC2844829.

28. Desrois M, Sidell RJ, Gauguier D, King LM, Radda GK, Clarke K. Initial steps of insulin signaling and glucose transport are defective in the type 2 diabetic rat heart. Cardiovasc Res. 2004; 61(2):288–96. Epub 2004/01/23. S0008636303007302 [pii]. PMID: 14736545.

29. Portha B, Serradas P, Bailbe D, Suzuki K, Goto Y, Giroix MH. Beta-cell insensitivity to glucose in the GK rat, a spontaneous nonobese model for type II diabetes. Diabetes. 1991; 40(4):486–91. Epub 1991/04/01. PMID: 2010050.

30. Desrois M, Clarke K, Lan C, Dalmasso C, Cole M, Portha B, et al. Upregulation of eNOS and unchanged energy metabolism in increased susceptibility of the aging type 2 diabetic GK rat heart to ischemic injury. Am J Physiol Heart Circ Physiol. 2010; 299(5):H1679–86. Epub 2010/08/24. ajpheart.00998.2009 [pii] doi: 10.1152/ajpheart.00998.2009 PMID: 20729402; PubMed Central PMCID: PMC2993220.

31. Goto Y, Kakizaki M, Masaki N. Production of spontaneous diabetic rats by repetition of selective breeding. Tohoku J Exp Med. 1976; 119(1):85–90. Epub 1976/05/01. PMID: 951706.

32. Goto Y, Suzuki K, Ono T, Sasaki M, Toyota T. Development of diabetes in the non-obese NIDDM rat (GK rat). Adv Exp Med Biol. 1988; 246:29–31. Epub 1988/01/01. PMID: 3074659.

33. Portha B. Programmed disorders of beta-cell development and function as one cause for type 2 diabetes? The GK rat paradigm. Diabetes Metab Res Rev. 2005; 21(6):495–504. Epub 2005/06/01. doi: 10.1002/dmrr.566 PMID: 15926190.

34. Giannesini B, Izquierdo M, Le Fur Y, Cozzone PJ, Fingerle J, Himber J, et al. New experimental setup for studying strictly noninvasively skeletal muscle function in rat using 1H-magnetic resonance (MR) imaging and 31P-MR spectroscopy. Magn Reson Med. 2005; 54(5):1058–64. Epub 2005/09/30. doi: 10.1002/mrm.20637 PMID: 16193467.

35. Mattei JP, Fur YL, Cuge N, Guis S, Cozzone PJ, Bendahan D. Segmentation of fascias, fat and muscle from magnetic resonance images in humans: the DISPIMAG software. MAGMA. 2006; 19(5):275–9. Epub 2006/09/28. doi: 10.1007/s10334-006-0051-1 PMID: 17004065.

36. Vanhamme L, van den Boogaart A, Van Huffel S. Improved method for accurate and efficient quantification of MRS data with use of prior knowledge. J Magn Reson. 1997; 129(1):35–43. Epub 1998/01/04. S1090780797912441 [pii]. PMID: 9405214.

37. Arnold DL, Matthews PM, Radda GK. Metabolic recovery after exercise and the assessment of mitochondrial function in vivo in human skeletal muscle by means of 31P NMR. Magn Reson Med. 1984; 1(3):307–15. Epub 1984/09/01. PMID: 6571561.

38. Kemp GJ, Radda GK. Quantitative interpretation of bioenergetic data from 31P and 1H magnetic resonance spectroscopic studies of skeletal muscle: an analytical review. Magn Reson Q. 1994; 10(1):43–63. Epub 1994/03/01. PMID: 8161485.

39. Amara CE, Shankland EG, Jubrias SA, Marcinek DJ, Kushmerick MJ, Conley KE. Mild mitochondrial uncoupling impacts cellular aging in human muscles in vivo. Proc Natl Acad Sci USA. 2007; 104(3):1057–62. PMID: 17215370.

40. Giannesini B, Izquierdo M, Le Fur Y, Cozzone PJ, Bendahan D. In vivo reduction in ATP cost of contraction is not related to fatigue level in stimulated rat gastrocnemius muscle. J Physiol (Lond). 2001; 536(3):905–15. PMID: 11691882

41. Thompson CH, Kemp GJ, Sanderson AL, Radda GK. Skeletal muscle mitochondrial function studied by kinetic analysis of postexercise phosphocreatine resynthesis. J Appl Physiol. 1995; 78(6):2131–9. PMID: 7665409.

42. Roth K, Weiner MW. Determination of cytosolic ADP and AMP concentrations and the free energy of ATP hydrolysis in human muscle and brain tissues with 31P NMR spectroscopy. Magn Reson Med. 1991; 22(2):505–11. Epub 1991/12/01. PMID: 1812384.

43. Hochachka PW, Mommsen TP. Protons and anaerobiosis. Science. 1983; 219(4591):1391–7. Epub 1983/03/25. PMID: 6298937.

44. Wolfe CL, Gilbert HF, Brindle KM, Radda GK. Determination of buffering capacity of rat myocardium during ischemia. Biochim Biophys Acta. 1988; 971(1):9–20. PMID: 2841984

45. Adams GR, Foley JM, Meyer RA. Muscle buffer capacity estimated from pH changes during rest-to-work transitions. J Appl Physiol. 1990; 69(3):968–72. PMID: 2246184

46. Wang X, DuBois DC, Cao Y, Jusko WJ, Almon RR. Diabetes disease progression in Goto-Kakizaki rats: effects of salsalate treatment. Diabetes Metab Syndr Obes. 2014; 7:381–9. Epub 2014/08/15. doi: 10.2147/DMSO.S65818 dmso-7-381 [pii]. PMID: 25120374; PubMed Central PMCID: PMC4128793.

47. Bisbis S, Bailbe D, Tormo MA, Picarel-Blanchot F, Derouet M, Simon J, et al. Insulin resistance in the GK rat: decreased receptor number but normal kinase activity in liver. Am J Physiol. 1993; 265(5 Pt 1):E807–13. Epub 1993/11/01. PMID: 8238507.

48. Farese RV, Standaert ML, Yamada K, Huang LC, Zhang C, Cooper DR, et al. Insulin-induced activation of glycerol-3-phosphate acyltransferase by a chiro-inositol-containing insulin mediator is defective in adipocytes of insulin-resistant, type II diabetic, Goto-Kakizaki rats. Proc Natl Acad Sci U S A. 1994; 91 (23):11040–4. Epub 1994/11/08. PMID: 7972005; PubMed Central PMCID: PMC45162.

49. Wallimann T, Wyss M, Brdiczka D, Nicolay K, Eppenberger HM. Intracellular compartmentation, structure and function of creatine kinase isoenzymes in tissues with high and fluctuating energy demands: the 'phosphocreatine circuit' for cellular energy homeostasis. Biochem J. 1992; 281 (Pt 1):21–40. Epub 1992/01/01. PMID: 1731757; PubMed Central PMCID: PMC1130636.

50. Prompers JJ, Wessels B, Kemp GJ, Nicolay K. MITOCHONDRIA: investigation of in vivo muscle mitochondrial function by 31P magnetic resonance spectroscopy. Int J Biochem Cell Biol. 2014; 50:67–72. Epub 2014/02/27. doi: 10.1016/j.biocel.2014.02.014 S1357-2725(14)00057-0 [pii]. PMID: 24569118.

51. Jorgensen W, Jelnes P, Rud KA, Hansen LL, Grunnet N, Quistorff B. Progression of type 2 diabetes in GK rats affects muscle and liver mitochondria differently: pronounced reduction of complex II flux is observed in liver only. Am J Physiol Endocrinol Metab. 2012; 303(4):E515–23. Epub 2012/06/21. doi: 10.1152/ajpendo.00103.2012 ajpendo.00103.2012 [pii]. PMID: 22713504.

52. Boutilier RG. Mechanisms of cell survival in hypoxia and hypothermia. J Exp Biol. 2001; 204(Pt 18):3171–81. Epub 2001/10/03. PMID: 11581331.

53. Padilla DJ, McDonough P, Behnke BJ, Kano Y, Hageman KS, Musch TI, et al. Effects of Type II diabetes on capillary hemodynamics in skeletal muscle. Am J Physiol Heart Circ Physiol. 2006; 291(5): H2439–44. Epub 2006/07/18. 00290.2006 [pii] doi: 10.1152/ajpheart.00290.2006 PMID: 16844923.

54. Hochachka PW, McClelland GB. Cellular metabolic homeostasis during large-scale change in ATP turnover rates in muscles. J Exp Biol. 1997; 200(Pt 2):381–6. Epub 1997/01/01. PMID: 9050247.

55. Lanza IR, Bhagra S, Nair KS, Port JD. Measurement of human skeletal muscle oxidative capacity by 31P-MR spectroscopy: a cross-validation with in vitro measurements. J Magn Reson Imaging. 2011; 34 (5):1143–50. Epub 2011/10/19. doi: 10.1002/jmri.22733 PMID: 22006551; PubMed Central PMCID: PMC3201762.

56. Petersen KF, Dufour S, Shulman GI. Decreased insulin-stimulated ATP synthesis and phosphate transport in muscle of insulin-resistant offspring of type 2 diabetic parents. PLoS Med. 2005; 2(9):e233. Epub 2005/08/11. 05-PLME-RA-0003R2 [pii] doi: 10.1371/journal.pmed.0020233 PMID: 16089501; PubMed Central PMCID: PMC1184227.

57. Hinder LM, Vivekanandan-Giri A, McLean LL, Pennathur S, Feldman EL. Decreased glycolytic and tricarboxylic acid cycle intermediates coincide with peripheral nervous system oxidative stress in a murine model of type 2 diabetes. J Endocrinol. 2013; 216(1):1–11. Epub 2012/10/23. doi: 10.1530/JOE-12-0356 JOE-12-0356 [pii]. PMID: 23086140.

58. Giannesini B, Cozzone PJ, Bendahan D. Non-invasive investigations of muscular fatigue: metabolic and electromyographic components. Biochimie. 2003; 85(9):873–83. PMID: 14652176.

59. Sleigh A, Raymond-Barker P, Thackray K, Porter D, Hatunic M, Vottero A, et al. Mitochondrial dysfunction in patients with primary congenital insulin resistance. J Clin Invest. 2011; 121(6):2457–61. Epub 2011/05/11. doi: 10.1172/JCI46405 46405 [pii]. PMID: 21555852; PubMed Central PMCID: PMC3104774.

60. Murakawa Y, Zhang W, Pierson CR, Brismar T, Ostenson CG, Efendic S, et al. Impaired glucose tolerance and insulinopenia in the GK-rat causes peripheral neuropathy. Diabetes Metab Res Rev. 2002; 18(6):473–83. Epub 2002/12/07. doi: 10.1002/dmrr.326 PMID: 12469361.

61. Allen MD, Choi IH, Kimpinski K, Doherty TJ, Rice CL. Motor unit loss and weakness in association with diabetic neuropathy in humans. Muscle Nerve. 2013; 48(2):298–300. Epub 2013/05/01. doi: 10.1002/mus.23792 PMID: 23629918.

62. Andersen H, Gadeberg PC, Brock B, Jakobsen J. Muscular atrophy in diabetic neuropathy: a stereological magnetic resonance imaging study. Diabetologia. 1997; 40(9):1062–9. Epub 1997/09/23. doi: 10.1007/s001250050788 PMID: 9300243.

63. Greenman RL, Khaodhiar L, Lima C, Dinh T, Giurini JM, Veves A. Foot small muscle atrophy is present before the detection of clinical neuropathy. Diabetes Care. 2005; 28(6):1425–30. Epub 2005/05/28. 28/6/1425 [pii]. PMID: 15920063; PubMed Central PMCID: PMC1224714.

64. Huang J, Wang J, Gu L, Bao J, Yin J, Tang Z, et al. Effect of a low-protein diet supplemented with ketoacids on skeletal muscle atrophy and autophagy in rats with type 2 diabetic nephropathy. PLoS One. 2013; 8(11):e81464. Epub 2013/12/05. doi: 10.1371/journal.pone.0081464 PONE-D-13-20703 [pii]. PMID: 24303049; PubMed Central PMCID: PMC3841136.